Toward achieving flexible and high sensitivity hexagonal boron nitride neutron detectors

A. Maity, S. J. Grenadier, J. Li, J. Y. Lin, and H. X. Jiang[a)]
Department of Electrical and Computer Engineering, Texas Tech University, Lubbock, Texas 79409, USA

(Received 9 May 2017; accepted 8 July 2017; published online 20 July 2017)

Hexagonal boron nitride (h-BN) detectors have demonstrated the highest thermal neutron detection efficiency to date among solid-state neutron detectors at about 51%. We report here the realization of h-BN neutron detectors possessing one order of magnitude enhancement in the detection area but maintaining an equal level of detection efficiency of previous achievement. These 3 mm × 3 mm detectors were fabricated from 50 μm thick freestanding and flexible ^{10}B enriched h-BN (h-^{10}BN) films, grown by metal organic chemical vapor deposition followed by mechanical separation from sapphire substrates. Mobility-lifetime results suggested that holes are the majority carriers in unintentionally doped h-BN. The detectors were tested under thermal neutron irradiation from californium-252 (^{252}Cf) moderated by a high density polyethylene moderator. A thermal neutron detection efficiency of ~53% was achieved at a bias voltage of 200 V. Conforming to traditional solid-state detectors, the realization of h-BN epilayers with enhanced electrical transport properties is the key to enable scaling up the device sizes. More specifically, the present results revealed that achieving an electrical resistivity of greater than 10^{14} Ω·cm and a leakage current density of below 3×10^{-10} A/cm^2 is needed to fabricate large area h-BN detectors and provided guidance for achieving high sensitivity solid state neutron detectors based on h-BN. *Published by AIP Publishing.* [http://dx.doi.org/10.1063/1.4995399]

Special nuclear materials (SNMs) such as Plutonium-239 (^{239}Pu) emit fast neutrons (^1_0n) through fission reactions. Thus, an effective way to detect SNMs is to detect neutrons emitted by SNMs. Detection systems based on hellium-3 (^3_2He) gas detectors have been widely deployed at the ports of the entry of the USA for this purpose. Apart from being expensive, being a gas, ^3_2He contains very low atomic density corresponding to a long absorption length for thermal neutrons, making ^3_2He detectors bulky. Other shortcomings of ^3_2He detectors have a low Q value (~0.764 MeV), high ionization energy, and high voltage operation. Therefore, alternative solid-state detectors that have the performance of ^3_2He detectors without their drawbacks are highly sought-after technologies.[1–7] Hexagonal boron nitride (h-BN), a wide bandgap semiconductor material, has emerged as a promising candidate for thermal neutron detection in recent years[8–13] due to the fact that the isotope ^{10}B has a high capture cross-section (~3840 b = 3.84 × 10^{-21} cm^2) for thermal neutrons[14] and h-BN possesses a high boron density (~5.5 × 10^{22} cm^{-3}). A 100% ^{10}B enriched h-BN (h-^{10}BN) detector has a thermal neutron absorption length (λ) of only 47.3 μm.[12] Its large bandgap (~6.5 eV)[15–23] inherently renders intrinsic h-BN highly resistive, yielding detectors with extremely low leakage currents. Neutron detectors of 1 × 1 mm^2 in size fabricated from h-^{10}BN epilayers have demonstrated the highest thermal neutron detection efficiency to date among solid-state neutron detectors at about 51%.[12]

However, scaling up to large area detectors is a necessary step for practical applications of h-BN neutron detectors. This is because the count rate (C_R) detected by using a detector (or the sensitivity of a detector) is proportional to its thermal neutron detection efficiency (η) and detection area (A), and for perpendicular neutron flux, C_R can be expressed as

$$C_R = \frac{N}{4\pi d^2}\eta A, \tag{1}$$

where N is the thermal neutron emission rate and d the distance between the detector and the neutron source. As an illustration, we consider the case of a 5 kg of Pu, which emits fast neutrons at a rate of ~3 × 10^5 neutrons/s with an average energy of ~1 MeV.[24] To detect such a source at targeted distances of 0.8, 2.4, and 7.7 m with a desired count rate of 1 n/s, it will require detectors with areas of 1, 10, and 100 cm^2, respectively, assuming that these detectors have a thermal neutron detection efficiency of 50% and are working in conjunction with high density polyethylene (HDPE) moderators for converting fast neutrons to thermal neutrons with a 50% conversion efficiency. Therefore, scaling up the detector area while maintaining a high detection efficiency is a necessity for detecting SNMs. To address the detector size issue, detection systems generally incorporate arrays of smaller detectors. However, when arrays of smaller detectors are being implemented, it is necessary to gear each small detector with its own electronics in order to maximize the performance, which increases the system design complexity and cost. Therefore, detectors with a large area are still preferred. Based on other solid-state neutron detector technologies, a minimum device size of 1 cm^2 is desirable.[3,25]

Nevertheless, there are technical challenges in realizing large size neutron detectors, the chief of which are (a) increased leakage current, leading to the introduction of excessive noise, and (b) reduced maximum applicable bias voltage, leading to the reduction in the charge carrier collection efficiency. The presence of a high noise level in neutron

a)Email: hx.jiang@ttu.edu

detection affects the setting point of a low level discriminator, leading to a small signal to noise ratio which could exclude a fraction of the actual counts from being detected. The equivalent noise charge in a simple CR-RC shaper at a fixed integration and differentiation time constant τ_c can be written as[26]

$$\langle Q_n^2 \rangle = 0.924 \left[2eI_d\tau_c + \frac{4K_BT}{R_b}\tau_c + e_n^2\frac{C^2}{\tau_c} \right]. \quad (2)$$

Here, the "shot noise" in the first term increases with the detector's dark current I_d, which is proportional to the device area (A). The second term is the "thermal noise" contributed from the bias resistor R_b. K_B is Boltzmann's constant and T is the operating temperature (300 K). The last term in Eq. (2) depends on the equivalent input noise of the amplifier with a spectral density e_n and equivalent input capacitance C. Capacitances of h-BN detectors are smaller compared to other semiconductor neutron detectors due to a small dielectric constant of about 4 for h-BN.[27] Equation (2) clearly shows that simply scaling up the detection area by one order of magnitude using the same h-BN material would result in one order of magnitude increment in the detector's dark current and hence in the equivalent noise, which would degrade the detection efficiency. The only way to realize a larger size and high efficiency neutron detector is to further enhance the electrical transport properties through improvement in material quality so that I_d and the required bias voltage would remain relatively low regardless of the area increment.

The bandgap of h-BN is about 6.5 eV (Refs. 15–23), and hence, intrinsic h-BN is almost an insulator with an expected electrical resistivity exceeding $10^{20}\,\Omega$ cm. However, the highest resistivity of unintentionally doped h-BN epilayers produced so far is about $5 \times 10^{13}\,\Omega$ cm,[10–12] implying that a significant improvement is anticipated through the optimization of epitaxial growth processes. Our recent studies have shown that growing h-BN epilayers in nitrogen-rich growth conditions can reduce the density of undesired native and point defects such as nitrogen vacancies (V_N) and carbon impurities occupying nitrogen sites (C_N).[28,29] Here, we report the realization of h-^{10}BN neutron detectors possessing one order of magnitude enhancement in the detection area (3 mm × 3 mm) over that of the previous achievement (1 mm × 1 mm) while upholding the same level of high detection efficiency.

^{10}B enriched h-BN (h-^{10}BN) epilayers were grown by metal organic chemical vapor deposition on c-plane sapphire substrates of 4-in. in diameter. Trimethylboron (TMB) with a vendor specified ^{10}B isotope enrichment of 99.9% and ammonia (NH_3) were used as the precursors for the growth of h-^{10}BN epilayers. Sample A (43 μm thick) has been previously used to fabricate 1 mm × 1 mm neutron detectors with a detection efficiency of about 51%,[12] whereas sample B has a layer thickness of 50 μm. Photoluminescence (PL) measurements revealed that the donor-acceptor pair transition at about 4.1 eV (Ref. 28) associated with V_N donors and C_N deep level acceptors is stronger in sample A than in sample B, indicating that the concentrations of V_N and C_N in sample A are higher than those in sample B. Therefore, sample B is expected to have a better overall material quality over that of sample A. Due to the nature of the layered structure of h-BN and the thermal expansion coefficient mismatch between h-BN and sapphire, free-standing h-^{10}BN wafers were obtained by mechanically separating h-^{10}BN from sapphire substrates, as shown in Fig. 1(a). The flexibility of free-standing h-BN films is demonstrated in Fig. 1(b). Free-standing h-BN wafers were easily sliced into desired dimensions. E-beam evaporation was used to deposit metal contacts consisting of a bi-layer of Ni (10 nm)/Au (20 nm) on both sides of the free-standing h-^{10}BN film to form "photoconductor-type" of detectors, as shown schematically in the inset of Fig. 2(a). $1 \times 1\,\text{mm}^2$ detectors were fabricated from sample A and sample B, labeled as D1 and D2, respectively, to assess directly the effects of the material quality on the performance of the fabricated detectors. A $3 \times 3\,\text{mm}^2$ detector (D3) was fabricated from sample B. The device fabrication processes for sample A and sample B were kept identical. Figures 2(a) and 2(b) show the comparison of dark current-voltage (I-V) and dark current density-voltage (J-V) characteristics among detectors D1, D2, and D3. The dark current and current density values at 500 V are listed in Table I, which shows that the dark current density of detector D1 fabricated from sample A is about 6 times higher than that of detectors D2 and D3 fabricated from sample B, whereas the

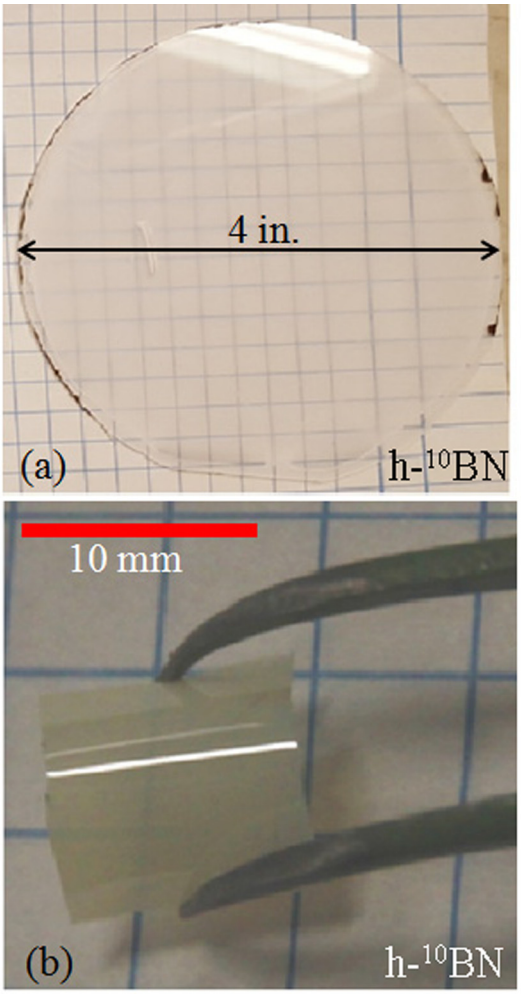

FIG. 1. (a) Photograph of a ^{10}B-enriched free standing h-BN wafer of 4-in. in diameter. (b) Photograph of a representative freestanding flexible h-^{10}BN film with a thickness of 50 μm.

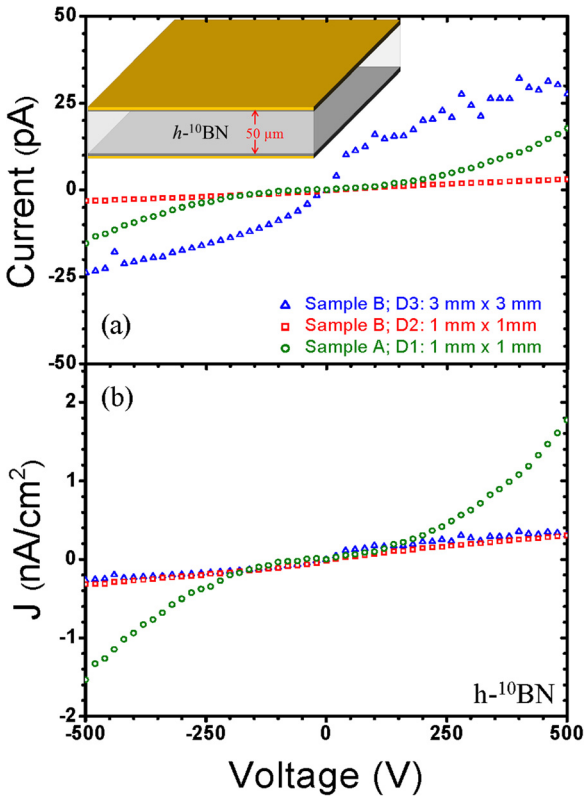

FIG. 2. Dark (a) I-V and (b) J-V characteristics of detector D1 ($1 \times 1\,mm^2$) fabricated from sample A ($43\,\mu m$ thick) and detectors D2 ($1 \times 1\,mm^2$) and D3 ($3 \times 3\,mm^2$) fabricated from sample B ($50\,\mu m$ thick). The inset shows the schematic of the cross-sectional view of these h-^{10}BN detectors.

measured resistivity (ρ) of sample B is about 5 times larger than that of sample A. Leakage current is a measure of the escape of electric current through defects/dislocations, and hence, a higher leakage current density also infers higher concentrations of defects and dislocations in sample A, consistent with the PL results.

For a given device dimension, enhancing the mobility-lifetime ($\mu\tau$) product would reduce the bias voltage (V) required for charge collection and the associated leakage current. This is because most charge carriers generated inside the detector can be collected at the electrodes when the condition of recombination time (τ) $\geq$ transit time (τ_t) is satisfied, i.e., $\mu\tau \geq L^2/V$ ($\tau_t = L/\mu E$, $E = V/L$),[10–12] where V is the applied voltage and L the transit length (the thickness of the detector). A deuterium UV lamp was used as a light source to illuminate one side of the detector. Due to the unique property of high optical absorption ($7 \times 10^5\,cm^{-1}$) of h-BN, above bandgap photons having a very short absorption length ($\lambda \sim 13\,nm$)[30,31] are completely absorbed within a few tens of layers of h-^{10}BN from the illuminated surface. Therefore, depending upon the polarity of the illuminated surface, a specific charge carrier (hole or electron) is selected for charge transport. The positively (negatively) biased illuminated surface collects photo-generated electrons (holes) and therefore allows only holes (electrons) to transport between the electrodes. Thus, photocurrent-voltage characteristics allow us to measure the $\mu\tau$-products for holes and electrons separately using Many's equation[32]

$$I_i(V) = I_{0,i}\left[\frac{V\mu_i\tau_i\left(1 - e^{-\frac{L^2}{V\mu_i\tau_i}}\right)}{L^2\left(1 + \frac{s_i L}{\mu_i V}\right)}\right], \quad (i = e,\ h). \tag{3}$$

Here, I_0 is the saturation current, and $\mu_e\tau_e$ ($\mu_h\tau_h$) and s_e (s_h) denote the mobility-lifetime product and surface recombination velocity for electrons (holes), respectively. The photocurrents in Fig. 3 are fitted with Eq. (3) to obtain $\mu_e\tau_e$ and $\mu_h\tau_h$ products, and the results are summarized in Table I, which reveals that $\mu_h\tau_h$ is greater than $\mu_e\tau_e$ for both samples. This is consistent with our understanding that although μ_h and μ_e are comparable, τ_h is larger than τ_e, implying that holes act as the majority carriers in unintentionally doped h-BN.[12] As shown in Table I, for the $1 \times 1\,mm^2$ devices (D1 and D2), the measured $\mu\tau$ values are larger for sample B than those of sample A. Therefore, the $\mu\tau$ characterization results again revealed an overall improvement in the material quality of sample B over sample A, consistent with the resistivity, leakage current density, and PL results. It should be noted that characterizing $\mu\tau$ products using a contactless geometry[32] which can minimize the contact effects is highly desirable in the future. However, the measured $\mu\tau$ values are lower for the 3 mm $\times$ 3 mm device (D3). This reduction in $\mu\tau$ products with the increasing device area is not expected if h-BN epilayers were perfectly homogenous. We believe that the observed reduction in $\mu\tau$ values in larger area devices arises primarily from crystalline imperfections and non-uniform distribution of defects across the h-BN wafer and the fact that the number of charge traps is proportional to the device area. This empirically observed reduction in $\mu\tau$ products with the increasing device area presents the major challenge for achieving large area detectors at this stage. The results clearly indicate that further improvements in epitaxial growth processes leading to materials with enhanced crystalline quality and reduced defect densities are needed.

The detection of thermal neutrons by h-^{10}BN detectors is via the following nuclear reactions:[14]

$$^{10}_{5}B + {}^{1}_{0}n = {}^{7}_{3}Li^{*}\,(0.84\,MeV) + {}^{4}_{2}\alpha^{*}\,(1.47\,MeV) \times [94\%\ excited\ state], \tag{4a}$$

TABLE I. Comparison of electrical transport properties among detector D1 ($1 \times 1\,mm^2$) fabricated from sample A ($43\,\mu m$ thick) and detectors D2 ($1 \times 1\,mm^2$) and D3 ($3 \times 3\,mm^2$) fabricated from sample B ($50\,\mu m$ thick).

Sample	Device	d (μm)	A (mm^2)	I_d (pA) at 500 V	J_d (nA/cm^2) at 500 V	ρ (10^{14}) (Ω)	$\mu_h\tau_h$ (10^{-5}) (cm^2/V)	I_{oh} (pA)	$\mu_e\tau_e$ (10^{-5}) (cm^2/V)	I_{oe} (pA)
B	D3	50	3 × 3	24(±1)	0.27(±0.02)	3.8(±0.2)	1.0(±0.1)	11(±0.2)	0.20(±0.01)	38(±0.4)
B	D2	50	1 × 1	3.0(±0.1)	0.30(±0.01)	3.3(±0.1)	2.3(±0.7)	21(±0.4)	1.3(±0.2)	2.2(±0.1)
A	D1	43	1 × 1	18(±1.0)	1.8(±0.1)	0.65(±0.04)	1.7(±0.7)	8.0(±0.1)	0.9(±0.2)	4.3(±0.1)

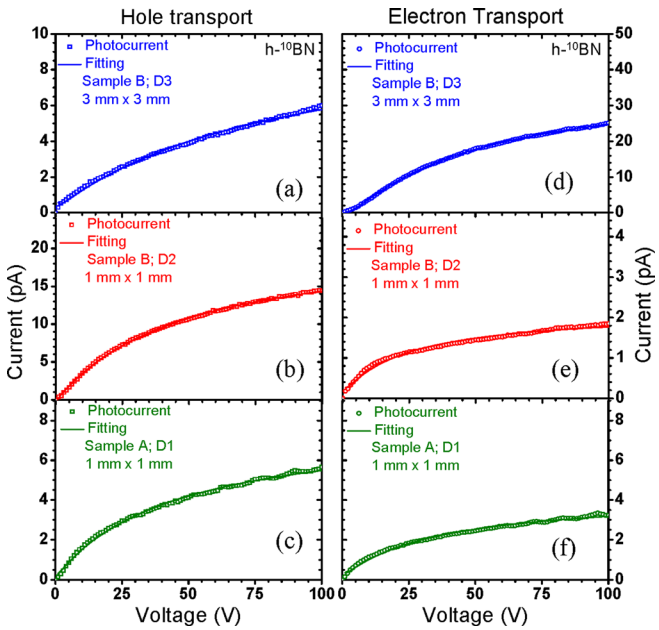

FIG. 3. Photocurrent-voltage characteristics favoring the hole transport for detectors (a) D3 ($3 \times 3\,mm^2$), (b) D2 ($1 \times 1\,mm^2$), and (c) D1 ($1 \times 1\,mm^2$). Photocurrent-voltage characteristics favoring the electron transport for detectors (d) D3 ($3 \times 3\,mm^2$), (e) D2 ($1 \times 1\,mm^2$), and (f) D1 ($1 \times 1\,mm^2$). The solid curves are the least squares fittings of Eq. (3) with experimental data.

$$^{10}_{5}B + {}^{1}_{0}n = {}^{7}_{3}Li\,(1.015\,\mathrm{MeV}) + {}^{4}_{2}\alpha\,(1.777\,\mathrm{MeV}) \times [6\%\ ground\ state]. \quad (4b)$$

The daughter particles $\left({}^{7}_{3}Li, {}^{4}_{2}\alpha\right)$ with high kinetic energies travel inside the material and lose their energies through ionization within a short distance ($\sim 5\,\mu m$ for α and $\sim 2\,\mu m$ for Li). An electric field was applied to extract the holes and electrons generated by $\left({}^{7}_{3}Li, {}^{4}_{2}\alpha\right)$ particles. A current pulse was obtained, which was integrated through a charge sensitive preamplifier (Cremat, Inc., model CR-110) with a gain of 1.4 V/pC to acquire a voltage pulse. This voltage pulse was further amplified and shaped in a Gaussian shaping amplifier (Cremat, Inc., model CR-200) with a shaping time of 2 μs (FWHM, 4.7 μs). A digital multi-channel analyzer (MCA) from Amptek (model 8000D) was used to obtain a pulse height spectrum from these voltage pulses. Neutrons are counted one at a time due to the very low rate of neutrons reaching the detector surface compared to the response time of the detection system. Detectors and corresponding electronics were shielded from external electromagnetic interference. A ^{252}Cf source with a radioactivity of 0.77 mCi ($\sim 3.29 \times 10^6$ n/s) in conjunction with a 1-in. thick HDPE moderator for converting fast neutrons into thermal neutrons was used as a thermal neutron source.[9–12,33] A pulse height spectrum under thermal neutron exposure for 15 min shown in Fig. 4 was obtained from the $3 \times 3\,mm^2$ detector (D3) at a bias of 200 V by placing the detector 60 cm from the ^{252}Cf source (or 57.5 cm from the front surface of the moderator). Exposure of h-^{10}BN detectors to Caesium-137 has already established the fact that they are irresponsive to γ photons because B and N are low atomic elements.[9–12]

A neutron spectrum was integrated above the highest channel of the dark spectrum to find the total number of thermal neutron counts. The count rate obtained in this way was

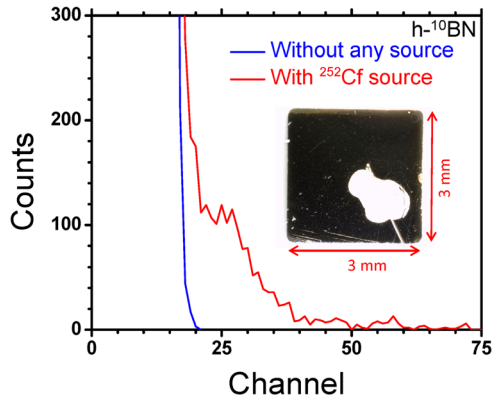

FIG. 4. Pulse height spectrum of detector D3 ($3 \times 3\,mm^2$ device fabricated from h-^{10}BN of 50 μm in thickness, sample B) measured under a bias voltage of 200 V for 15 min. The red curve represents the response under thermal neutron irradiation from the ^{252}Cf-HDPE moderator at a distance of 60 cm from the source. To determine the "dark" or electronic noise level at this distance, another measurement was conducted for 15 min at the same bias voltage in the absence of any source (blue curve). The inset shows an optical image of detector D3.

1.7 ± 0.02 n/s, giving a count rate per unit area $C_{BN} = 18.4 \pm 0.2$ n/s cm^2 for the $3 \times 3\,mm^2$ h-^{10}BN detector (D3). A certified ^{6}LiF filled Si microstructured neutron detector (MSND Domino™ V4 with a detection area of 4 cm^2 from Radiation Detection Technology, Inc.) with a specified thermal neutron detection efficiency of $\eta_{MSND} = 30\ (\pm 1)\%$ was used to calibrate the detection efficiency of h-^{10}BN detectors by placing it at the same position as the h-^{10}BN detector. A count rate of about 42.1 ± 0.1 n/s was obtained from MSND, providing $C_{MSND} = 10.5 \pm 0.03$ n/s cm^2. From the ratios of the detection efficiencies and count rates per unit area between h-^{10}BN and MSND detectors,[12] the thermal neutron detection efficiency for the $3 \times 3\,mm^2$ h-^{10}BN detector can be deduced to be $\eta_{BN} = (C_{BN}/C_{MSND}) \cdot \eta_{MSND} = 53\ (\pm 2)\%$.

The measured detection efficiency for D3 ($3 \times 3\,mm^2$ device) biased at 200 V is comparable to the previously reported efficiency of $\sim 51\%$ for a $1 \times 1\,mm^2$ detector biased at 400 V.[12] This reduction in the required bias voltage for obtaining an equal level of detection efficiency is again attributed to the improved material quality of sample B. The calculated absorption length (λ) for thermal neutrons in h-^{10}BN is $\sim 47.3\,\mu m$.[12] Thus, a 50 μm thick h-^{10}BN detector in principle can absorb $\sim 65.3\%$ of incident thermal neutrons, which infers that our $3 \times 3\,mm^2$ h-^{10}BN detector has attained a ratio of the measured to predicted efficiency of about 81% at a bias voltage of 200 V. The observed discrepancy between the measured and predicted efficiency can be accounted for by the imperfect charge collection efficiency due to the fact that the overall material quality of h-BN epilayers is still far-off from state-of-the-art and the possibility that the actual enrichment of the ^{10}B precursor used for the growth of h-^{10}BN epilayers is less than the specified value of 99.9%.

In summary, the attainment of free-standing 50 μm thick h-^{10}BN epilayers with reduced defect density and enhanced electrical transport properties has enabled the fabrication 3 mm × 3 mm neutron detectors with a detection efficiency of about 53%. The present results have provided useful insights into the realization of highly efficient large size h-^{10}BN neutron detectors for many practical applications.

The DOE NNSA SSAA program (DE-NA0002927) supported the research efforts on *h*-BN neutron detector fabrication. The study of the basic transport properties of *h*-BN is made possible by the support from ARO (W911NF-16-1-0268) and monitored by Dr. Michael Gerhold. Jiang and Lin are grateful to the AT&T Foundation for the support of Ed Whitacre and Linda Whitacre, Endowed chairs.

[1]Q. Shao, L. F. Voss, A. M. Conway, R. J. Nikolic, M. A. Dar, and C. L. Cheung, Appl. Phys. Lett. **102**, 063505 (2013).
[2]K.-C. Huang, R. Dahal, J. J.-Q. Lu, A. Weltz, Y. Danon, and I. B. Bhat, Nucl. Instrum. Methods Phys. Res., Sect. A **763**, 260 (2014).
[3]S. L. Bellinger, R. G. Fronk, W. J. McNeil, T. J. Sobering, and D. S. McGregor, IEEE Trans. Nucl. Sci. **59**, 167 (2012).
[4]A. M. Conway, R. J. Nikolic, and T. F. Wang, in *Proceedings of the International Semiconductor Device Research Conference* (IEEE, New York, 2007), p. 589.
[5]K. Osberg, N. Schemm, S. Balkir, J. O. Brand, M. S. Hallbeck, P. A. Dowben, and M. W. Hoffman, IEEE Sens. J. **6**, 1531 (2006).
[6]D. S. McGregor, T. C. Unruh, and W. J. McNeil, Nucl. Instrum. Methods Phys. Res., Sect. A **591**, 530 (2008).
[7]A. N. Caruso, J. Phys.: Condens. Matter **22**, 443201 (2010).
[8]J. Li, R. Dahal, S. Majety, J. Y. Lin, and H. X. Jiang, Nucl. Instrum. Methods Phys. Res., Sect. A **654**, 417 (2011).
[9]T. C. Doan, S. Majety, S. Grenadier, J. Li, J. Y. Lin, and H. X. Jiang, Nucl. Instrum. Methods Phys. Res., Sect. A **748**, 84 (2014).
[10]T. C. Doan, S. Majety, S. Grenadier, J. Li, J. Y. Lin, and H. X. Jiang, Nucl. Instrum. Methods Phys. Res., Sect. A **783**, 121 (2015).
[11]T. C. Doan, J. Li, J. Y. Lin, and H. X. Jiang, AIP Adv. **6**, 075213 (2016).
[12]A. Maity, T. C. Doan, J. Li, J. Y. Lin, and H. X. Jiang, Appl. Phys. Lett. **109**, 072101 (2016).
[13]K. Ahmed, R. Dahal, A. Weltz, J. J.-Q. Lu, Y. Danon, and I. B. Bhat, Appl. Phys. Lett. **110**, 023503 (2017).
[14]G. F. Knoll, *Radiation Detection and Measurement*, 4th ed. (John Wiley & Sons, 2010).
[15]B. Arnaud, S. Lebègue, P. Rabiller, and M. Alouani, Phys. Rev. Lett. **96**, 026402 (2006).
[16]B. Arnaud, S. Lebègue, P. Rabiller, and M. Alouani, Phys. Rev. Lett. **100**, 189702 (2008).
[17]L. Wirtz, A. Marini, and A. Rubio, Phys. Rev. Lett. **96**, 126104 (2006).
[18]L. Museur, G. Brasse, A. Pierret, S. Maine, B. Attal-Tretout, F. Ducastelle, A. Loiseau, J. Barjon, K. Watanabe, T. Taniguchi, and A. Kanaev, Phys. Status Solidi RRL **5**, 214 (2011).
[19]L. Museur, E. Feldbach, and A. Kanaev, Phys. Rev. B **78**, 155204 (2008).
[20]K. Watanabe and T. Tanniguchi, Phys. Rev. B **79**, 193104 (2009).
[21]M. G. Silly, P. Jaffrennou, J. Barjon, J. S. Lauret, F. Ducastelle, A. Loiseau, E. Obraztsova, B. Attal-Tretout, and E. Rosencher, Phys. Rev. B **75**, 085205 (2007).
[22]X. K. Cao, B. Clubine, J. H. Edgar, J. Y. Lin, and H. X. Jiang, Appl. Phys. Lett. **103**, 191106 (2013).
[23]T. C. Doan, J. Li, J. Y. Lin, and H. X. Jiang, Appl. Phys. Lett. **109**, 122101 (2016).
[24]R. C. Byrd, J. M. Moss, W. C. Priedhorsky, C. A. Pura, G. W. Richter, K. J. Saeger, W. R. Scarlett, S. C. Scott, and R. L. Wagner, Jr., IEEE Sens. J. **5**, 593 (2005).
[25]S. L. Bellinger, R. G. Fronk, T. J. Sobering, and D. S. McGregor, Appl. Radiat. Isot. **70**, 1121 (2012).
[26]H. G. Spieler and E. E. Haller, IEEE Trans. Nucl. Sci. **32**, 419 (1985).
[27]A. J. Gatesman, R. H. Giles, and J. Waldman, in *1991 MRS Fall Meeting, Symposium G-Wide Band-Gap Semiconductors* (Mater. Res. Soc. Symp. Proc., 1992), Vol. **242**, p. 623.
[28]X. Z. Du, J. Li, J. Y. Lin, and H. X. Jiang, Appl. Phys. Lett. **106**, 021110 (2015).
[29]X. Z. Du, J. Li, J. Y. Lin, and H. X. Jiang, Appl. Phys. Lett. **108**, 052106 (2016).
[30]T. Sugino, K. Tanioka, S. Kawasaki, and J. Shirafuji, Jpn. J. Appl. Phys., Part 2 **36**, L463 (1997).
[31]J. Li, S. Majety, R. Dahal, W. P. Zhao, J. Y. Lin, and H. X. Jiang, Appl. Phys. Lett. **101**, 171112 (2012).
[32]A. Many, J. Phys. Chem. Solids **26**, 575 (1965).
[33]J. Clinton, "Optimization and characterization of a novel shelf powered solid state neutron detector," Ph.D. thesis, Rensselaer Polytechnic Institute, New York, USA, 2011, Chap. 3, pp. 73–78.